J|A|C|S ARTICLES

Published on Web 12/02/2010

Surface Chemistry of InP Quantum Dots: A Comprehensive Study

Arnaud Cros-Gagneux,[†] Fabien Delpech,*[,†] Céline Nayral,*[,†] Alfonso Cornejo,[†] Yannick Coppel,[‡] and Bruno Chaudret*[†,‡]

Université de Toulouse; INSA, UPS, CNRS; LPCNO (Laboratoire de Physique et Chimie des Nano-Objets), 135 avenue de Rangueil, F-31077 Toulouse, France, and Laboratoire de Chimie de Coordination, UPR-CNRS 8241, 205 route de Narbonne, 31077 Toulouse Cedex, France

Received May 29, 2010; E-mail: fabien.delpech@insa-toulouse.fr; celine.nayral@insa-toulouse.fr

Abstract: Advanced ^{1}H, ^{13}C, and ^{31}P solution and solid-state NMR studies combined with IR spectroscopy were used to probe, at the molecular scale, the composition and the surface chemistry of indium phosphide (InP) quantum dots (QDs) prepared via a non-coordinating solvent strategy. This nanomaterial can be described as a core−multishell object: an InP core, with a zinc blende bulk structure, is surrounded first by a partially oxidized surface shell, which is itself surrounded by an organic coating. This organic passivating layer is composed, in the first coordination sphere, of tightly bound palmitate ligands which display two different bonding modes. A second coordination sphere includes an unexpected dialkyl ketone and residual long-chain non-coordinating solvents (ODE and its isomers) which interact through weak intermolecular bonds with the alkyl chains of the carboxylate ligands. We show that this ketone is formed during the synthesis process via a decarboxylative coupling route and provides oxidative conditions which are responsible for the oxidation of the InP core surface. This phenomenon has a significant impact on the photoluminescence properties of the as-synthesized QDs and probably accounts for the failure of further growth of the InP core.

Introduction

Because of their unique size- and shape-dependent electronic and optical properties, semiconductor nanocrystals (NCs) (often termed quantum dots, QDs) have sparked a considerable interest for both fundamental and technological issues across many scientific disciplines. Representative examples are tunable emitters for biolabeling, lasers, light emitting diodes, and solar cells.[1] This has stimulated the development of a large number of procedures leading to nano-objects of increased complexity in terms of shape (rod, wire, multipods),[2] composition,[3] core−multishell structure,[4] or multifunctionality.[5] Many of these successes have been obtained thanks to the development of ligand (or surfactant)-controlled growth in hot organic solvent, a strategy which was first introduced in 1993 for CdSe NCs by Murray et al.[6] This synthetic route is based on the reaction of highly reactive species in media where surfactants play an essential role in the final shape, size, and stability of the desired nanomaterial. This aspect is now well-understood and has been rationalized in terms of dynamic coordination, with sometimes face-selective binding that leads to the formation of anisotropic crystal shapes.[2] The capping ligands also have a crucial role in the optical properties of the as-synthesized QDs. They interact electronically with surface sites and may sometimes passivate dangling bonds at the surface.[7] However, the electronic interactions of these molecules remain difficult to control, and passivation is often incomplete. This has led to the preparation of a second generation of QDs, i.e., core−shell structure NCs, in which the deposition of an inorganic shell insulates the core from the surface both physically and electronically. Compared to organically passivated NCs, the shelling provides significant improvements in the fluorescence quantum yields and stability against photo-oxidation. Moreover, the luminescence efficiency and the band edge lifetimes of the resulting core−shell structures were still found to depend on the ligands coordinated to the surface of the shell, charge carriers still having access to the particle surface despite the presence of a thick (2.2 nm) shell.[8]

Progress has also been achieved in the generalization of this approach to other materials such as IV−VI, III−V, and in particular InP-based QDs. The latter material has been identified as the most promising alternative to the ubiquitous CdSe NCs because of its broader emission color range and the lack of intrinsic toxicity as is associated with CdSe. However, the synthesis of InP QDs proves to be much trickier, and developments remain one step behind compared to the II−VI counterparts. InP particles were initially prepared by following a pathway adapted from the method established for cadmium

[†] Laboratoire de Physique et Chimie des Nano-Objets, Université de Toulouse.

[‡] Laboratoire de Chimie de Coordination, CNRS.

(1) Talapin, D. V.; Lee, J.-S.; Kovalenko, M. V.; Shevchenko, E. V. *Chem. Rev.* **2010**, *110*, 389–458.
(2) Yin, Y.; Alivisatos, A. P. *Nature* **2005**, *437*, 664–670.
(3) Allen, P. M.; Bawendi, M. G. *J. Am. Chem. Soc.* **2008**, *130*, 9240–9241.
(4) Jing, P.; Zheng, J.; Ikezawa, M.; Liu, X.; Lv, S.; Kong, X.; Zhao, J.; Masumoto, Y. *J. Phys. Chem. C* **2009**, *113*, 13545–13550.
(5) Zeng, H.; Sun, S. H. *Adv. Funct. Mater.* **2008**, *18*, 391–400.
(6) Murray, C. B.; Norris, D. J.; Bawendi, M. G. *J. Am. Chem. Soc.* **1993**, *115*, 8707–8715.
(7) Bullen, C.; Mulvaney, P. *Langmuir* **2006**, *22*, 3007–3013.
(8) Van Embden, J.; Jasieniak, J.; Mulvaney, P. *J. Am. Chem. Soc.* **2009**, *131*, 14299–14309.

chalcogenide NCs,[6] but longer reaction times (3−7 days) and size-selective precipitation procedures were necessary to yield well-crystallized InP particles displaying a narrow size distribution. Interestingly, the dynamics and the energetics of ligand exchange were studied in detail and gave a deep insight into surface−ligand and ligand−ligand interactions.[9,10] However, those works were limited to the fine description of the interplay between capping ligands (TOP/TOPO) and InP NCs and did not go further toward an understanding of the reaction pathways. More recently, significant improvements to the synthetic route have been achieved. Peng at al. reported a new strategy using a non-coordinating solvent, 1-octadecene (ODE), and fatty acids as ligands instead of a TOP/TOPO mixture.[11] This "greener" approach provides a fast and controllable reaction, yielding high-quality InP QDs without the need for a size-selective precipitation procedure. Further significant achievements, like one-pot synthesis of highly luminescent core−shell InP/ZnS without precursor injection, were also based on the use of ODE as solvent and long-chain carboxylic acids as ligands.[12,13] The use of additional compounds (fatty amines, zinc carboxylate) has also been shown to be beneficial for the ease of synthesis and the properties of these particles.[12−16] Thus, the chemistry of InP NCs has reached a level of maturity allowing the design of controlled InP-based NCs in terms of crystallinity, composition, and complex multishell structures. Very recently, in order to understand the broad size distributions in current InP QDs synthesis, Bawendi et al. have provided important mechanistic insights supporting a ripening growth in preparations involving a mixture of amine and acid ligands.[17] However, in general, the underlying mechanistic processes are still poorly understood, the studies being essentially focused on improving the optical properties through fine-tuning the experimental parameters.

Herein, we report a comprehensive study on the compositional characteristics, including the surface chemistry, of InP QDs prepared in non-coordinating solvents. We will, in particular, show that, besides the classical role of capping ligand, palmitic acid is also involved in an organic side reaction and that species which are not initially present but are formed *in situ* during the reaction course have a key role in the chemical features (e.g., QDs growth inhibition) as well as the optical characteristics of the as-synthesized InP NCs.

Experimental Section

Chemicals. Indium acetate ($In(OAc)_3$, ≥99.99%), palmitic acid (PA, ≥99.0%), elemental sulfur (≥99.98%), anhydrous cadmium acetate (≥99,99%), methanol (≥99.0%), and 1-octadecene (ODE, ≥90%, technical grade) were purchased from Sigma-Aldrich. Trimethylindium (≥99.99%), and tris(trimethylsilyl)phosphine ($P(TMS)_3$, ≥98.0%) were purchased from Strem. ^{13}C═O-enriched palmitic acid (≥99.0%) was purchased from Cambridge laboratory Inc. Hentriacontan-16-one (≥90.0%) was purchased from TCI Europe. Chloroform (PUREX, analysis grade), toluene, and acetone (RPE, analysis grade) were purchased from Carlo Erba. All reagents and solvents were dried, distilled, and degassed before use by using three freeze−pump−thaw cycles. All manipulations were carried out under an argon atmosphere using Schlenk tubes and vacuum line techniques, or in a glovebox.

Synthesis of InP Nanocrystals. InP NCs suspensions were synthesized according to a procedure described by Peng et al.,[11] using 0.7 mmol (204 mg) of indium acetate, 2.1 mmol (539 mg) of palmitic acid, and 0.35 mmol of tris(trimethylsilyl)phosphine (305 mg of 1 M solution in ODE) in 40 mL of ODE. Two washing procedures were used. In the standard procedure, the crude reaction mixture is mixed with 1 vol equiv of toluene and centrifuged (5000 rpm) for 10 min. The gray light precipitate is discarded. After evaporation of toluene under reduced pressure, the red supernatant is centrifuged (20 000 rpm) for 1 h, giving a red precipitate and red supernatant which is discarded. The red precipitate is dispersed in 2 mL of toluene, and 2 mL methanol is added, giving a cloudy solution that is centrifuged (5000 rpm) for 20 min. The colorless supernatant is discarded, and the red precipitate is washed again following the same procedure and then dried under reduced pressure and kept in a glovebox. In the acetone-based procedure, the crude reaction mixture is centrifuged (4000 rpm) for 5 min. The gray light precipitate is discarded. The red supernatant is mixed with 1 vol equiv of acetone and centrifuged (10 000 rpm) for 10 min. The transparent supernatant is discarded. One milliliter of $CHCl_3$ is added to the red oily precipitate, and then 15 mL of acetone is added, giving a cloudy solution that is centrifuged (10 000 rpm) for 10 min. This last washing step is repeated three more times, and the resulting red solid is dried under vacuum and kept in a glovebox.

Synthesis of InP/CdS Nanocrystals. The InP nanoparticles are prepared following the procedure described above. To 20 mL of the crude InP solution are added 37 mL of ODE, 0.49 mmol (213 mg) of cadmium acetate, and 0.49 mmol (15 mg) of elemental sulfur. The red-orange solution is stirred under reduced pressure for 10 min at 110 °C. The system is filled with argon and heated to 150 °C for 2 h. The solution becomes dark red and is cooled to room temperature. Isolation is done by following the acetone-based purification procedure.

Synthesis of Indium(III) Palmitate. A 100 mL Schlenk tube is loaded with 10 mL of toluene and 0.6 mmol (96 mg) of $InMe_3$. Another 100 mL Schlenk tube is loaded with 10 mL of toluene and 1.79 mmol (459 mg) of palmitic acid. The solution of $InMe_3$ is slowly added into the palmitic acid solution. Gas evolution is observed, and the solution mixture is kept under stirring for 30 min. The solution is then cooled to −35 °C and kept at this temperature overnight. The solution is filtered, yielding a white solid which is washed three times with 10 mL of acetone and dried under vacuum (225 mg, 41%). ^1H NMR ($CDCl_3$): δ 2.34 (br, 2H), 1.61 (br, 2H), 1.25 (br, 24H), 0.88 (t, 3H). ^{13}C NMR ($CDCl_3$): δ 31.92 (s, C14), 29.76 (br C6−C13), 29.40 (br, C4−C5), 25.19 (br, C3) 22.72 (s, C15), 14.12 (s, C16). IR: 2849−2916 (νC−H), 1527 (νCOO^- asym), 1443 (νCOO^- sym.) cm^{-1}. Anal. Calcd: C, 65.43; H, 10.64. Found: C, 66.94; H, 10.60.

Characterization of InP Nanocrystals. Samples for TEM analysis were prepared in a glovebox by slow evaporation of a drop of the colloidal solution deposited onto a carbon-covered copper grid. TEM analysis were performed at the Service Commun de Microscopie Electronique de l'Université Paul Sabatier (TEMSCAN) on a JEOL JEM 1011 electron microscope operating at 100 kV with a point resolution of 4.5 Å. The size distributions were determined by measuring ca. 300 particles using image J software.

Nuclear Magnetic Resonance Spectroscopy. 1D and 2D ^1H, ^{31}P, and ^{13}C NMR measurements in the liquid state were recorded on a Bruker Avance 500 spectrometer equipped with a 5 mm triple-resonance inverse Z-gradient probe (TBI ^1H, ^{31}P, BB). The InP QDs concentration range used in the dispersions is 1×10^{-4}−5×10^{-4} M. All the ^1H and ^{13}C signals were assigned on the basis of

(9) Hens, Z.; Moreels, I.; Martins, J. C. *ChemPhysChem* **2005**, *6*, 2578–2584.
(10) Moreels, I.; Martins, J. C.; Hens, Z. *ChemPhysChem* **2006**, *7*, 1028–1031.
(11) Battaglia, D.; Peng, X. *Nano Lett.* **2002**, *2*, 1027–1030, 9.
(12) Li, L.; Reiss, P. *J. Am. Chem. Soc.* **2008**, *130*, 11588–11589.
(13) Xu, S.; Ziegler, J.; Nann, T. *J. Mater. Chem.* **2008**, *18*, 2653–2656.
(14) Ryu, E.; Kim, S.; Jang, E.; Jun, S.; Jang, H.; Kim, B.; Kim, S.-W. *Chem. Mater.* **2009**, *21*, 573–575.
(15) Xie, R.; Battaglia, D.; Peng, X. *J. Am. Chem. Soc.* **2007**, *129*, 15432–15433.
(16) Protière, M.; Reiss, P. *Chem. Commun.* **2007**, 2417–2419.
(17) Allen, P. M.; Walker, B. J.; Bawendi, M. G. *Angew. Chem., Int. Ed.* **2010**, *49*, 760–762.

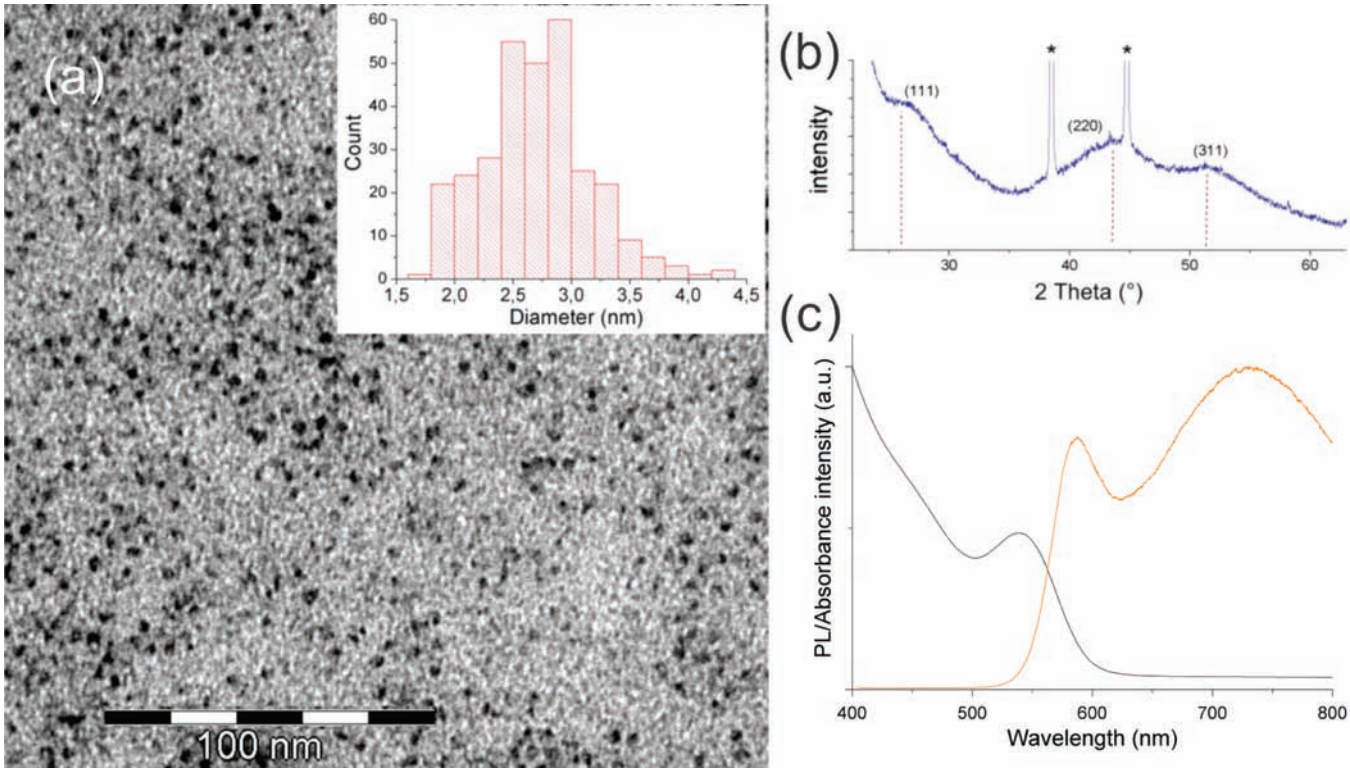

Figure 1. (a) TEM image, (b) X-ray diffractogram, and (c) UV−vis and PL spectra of InP QDs isolated using the standard purifying procedure. The inset of panel a shows the size distribution of the InP QDs.

chemical shifts, spin−spin coupling constants, splitting patterns, and signal intensities and by using $^{1}H-^{1}H$ COSY, $^{1}H-^{13}C$ HMQC, and $^{1}H-^{13}C$ HMBC experiments. The 2D NOESY measurements were done with a mixing time of 100 ms. All diffusion measurements were made using the stimulated echo pulse sequence. The recycle delay was adjusted to 3 s. The strength of the gradient was calibrated by measuring the self-diffusion of the residual HDO signal in a 100% D_2O sample at 298 K (1.90×10^{-9} m^2 s^{-1}). For 2D diffusion-ordered spectroscopy (DOSY), after Fourier transformation and baseline correction, the diffusion dimension was processed with the Bruker Topspin software package DOSY. Solid-state NMR experiments were recorded on a Bruker Avance 400 spectrometer equipped with a 4 mm probe. Samples were spun at 7 kHz at the magic angle using ZrO_2 rotors. For ^{1}H MAS, ^{13}C MAS, and ^{31}P MAS single-pulse experiments, a small flip angle (~30°) was used with recycle delays of 5, 10, and 60 s, respectively. ^{13}C CP/MAS and ^{31}P CP/MAS spectra were recorded with a recycle delay of 5 s and contact times of 2 and 3 ms, respectively. All the ^{13}C and ^{31}P NMR spectra were recorded under high-power proton decoupling conditions. All chemical shifts for ^{1}H and ^{13}C are relative to TMS. ^{31}P chemical shifts were referenced to an external 85% H_3PO_4 sample. $^{31}P\{^{1}H\}$ MAS NMR spectra were fully deconvoluted by dmfit software.[18]

Fourier Transform Infrared Spectroscopy. FT-IR spectra were recorded on a Perkin-Elmer Spectrum 100 FT-IR spectrometer (solid-state samples) and on a Perkin-Elmer Spectrum One spectrometer (solutions). Quantifications of the palmitic acid, the hentriacontan-16-one, and the palmitate ligand were achieved through the measurement of the surface (and/or of the height) of their respective carbonyl peaks in cyclohexane. Calibration was done using commercial batches for the palmitic acid and the hentriacontan-16-one and using indium palmitate prepared as described above. Analysis of the C−H vibration pattern was realized in $CDCl_3$.

(18) Massiot, D.; Fayon, F.; Capron, M.; King, I.; Le Calvé, S.; Alonso, B.; Durand, J. O.; Bujoli, B.; Gan, Z.; Hoatson, G. *Magn. Reson. Chem.* **2002**, *40*, 70–76.

UV−Visible Absorbance Spectroscopy. UV−vis spectra were measured by using a Perkin-Elmer Lambda 35 scanning spectrophotometer with the samples in 2 mm cells.

Photoluminescence Spectroscopy. PL spectra were acquired with the excitation laser centered at 402 nm (Nichia NLVH 3000E). The light was then dispersed by a monochromator (PI Acton SpectraPro 2500i). The detection was done at 90° by using a CDD camera (Spec-10:100 BR/LN). Acquisition was done by using Winspec32 software.

X-ray Diffraction Spectroscopy. XRD spectra were recorded on an MPD Pro Panalytical spectrometer using Cu Kα radiation. A powder of the sample was placed on a glass slide for the analysis.

Microanalysis. Elemental analyses were performed by the Service de microanalyses du Laboratoire de Chimie de Coordination (C, H, N) or by Antellis Co. (In, P).

Results

The InP nanoparticles were synthesized following the procedure previously reported by Peng et al.[11] with indium acetate ($In(OAc)_3$) and tris(trimethylsilyl)phosphine ($P(TMS)_3$) as the indium and phosphorus sources in the presence of palmitic acid ($CH_3(CH_2)_{14}COOH$) in 1-octadecene (ODE). The NCs were precipitated with a mixture of toluene and methanol by what we called the "standard purifying procedure" (see Experimental Section).

InP Core Characterization. TEM images showed dispersed spherical nanoparticles with sizes in the range of 2.7(0.5) nm (Figure 1). Elemental analysis by EDX and ICPMS confirmed the presence of indium and phosphorus in an approximate 2:1 ratio, consistent with the synthesis conditions and previous reports.[12] The optical properties (absorption and luminescence spectra) were found to be comparable to published results, with quantum yields (QY) close to 1%.[11,14,15,19] The excitonic emission peak is found around 590 nm, with a full width at half-maximum (fwhm) of only 55 nm, which is indicative of a narrow

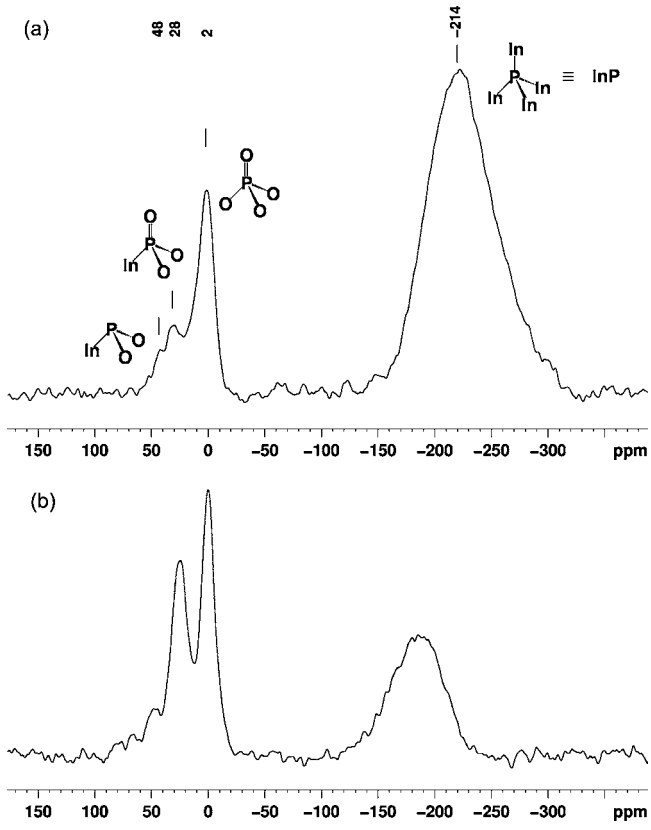

Figure 2. $^{31}P\{^1H\}$ (a) and CP $^1H-^{31}P$ (b) MAS NMR spectra of InP QDs isolated using the standard purifying procedure.

size distribution. In addition, an accompanying much broader and red-shifted luminescence is observed around 710 nm and is assigned to surface energy states of dangling indium bonds (Figure 1). The latter observation is inherent to the synthesis of InP NCs using indium carboxylate-based methodology.[13,16,19,20] Finally, a typical X-ray diffraction pattern of the zinc blende phase of InP is observed for the as-synthesized NCs, with diffraction peaks for lattice planes (111), (220), and (311) (Figure 1).[13,16,19,21] These features are fully consistent with the previous description of InP QDs prepared from indium carboxylate precursors that are now well-established. A deep understanding of their optical properties has also been gained, in particular in terms of quantum confinement and surface effects, to identify the origin of the two types of luminescence described above. However, and despite their importance, the surface structure and surface chemistry of these particles have so far received very little attention.[22] A MAS NMR study of these QDs was thus undertaken in order to clarify these issues.

When the InP QDs are analyzed with ^{31}P MAS NMR, the $^{31}P\{^1H\}$ NMR spectrum shows four resonances at δ 48, 28, 2, and -214 ppm in a 1:5:12:82 ratio (Figure 2 and see Supporting Information, Figure S1). The major one is broad and intense and lies in the high-field range typically found for nanoparticulate InP.[23] For instance, previous studies on TOPO-derived InP QDs have shown resonances with values varying from δ -192 to -178 for diameters of 2.5 and 4.5 nm, respectively. These resonances are shifted upfield with respect to bulk $In^{31}P$ (δ = -147 ppm, $\delta_{1/2}$ = 43 ppm). More interestingly, the line shape of the resonance at δ -214 is asymmetric and much broader ($\delta_{1/2}$ = 70 ppm) than the corresponding one in the bulk material.[23] This increased broadening is due to a distribution of chemical shifts and implies a manifold of capping ligand−NC bonding environment. The three other, minor resonances are related to phosphorus atoms located at or near (typically <0.5 nm) the surface of the QDs, as evidenced by the increased intensity in the cross-polarization (CP) $^1H-^{31}P$ MAS NMR spectrum (Figure 2b). The CP sequence, indeed, allows inferring spatial proximities between species at the interface, as it relies on dipolar coupling between different nuclear spins; this is thus a key NMR technique for investigating the organic and inorganic interfaces at a molecular level.[24] The significant increase in intensity for the 48, 28, and 2 ppm resonances in the CP $^1H-^{31}P$ MAS NMR spectrum shows unambiguously that these resonances arise from phosphorus species at the surface. Interestingly, exposure of the InP NCs to air results in enhancement of the intensity of the resonance at 2 ppm compared to the other resonances (see Supporting Information, Figure S2). Given the high sensitivity of InP to oxidation,[25] this result strongly supports that this resonance arises from surface oxidation. This is also consistent with previous ^{31}P NMR measurements on TOP/TOPO-passivated InP QDs: upon oxidation, an additional $^{31}PO_4-$surface resonance is observed.[23] The lower field resonance at 28 ppm is very comparable to that found in $In_{0.91}Ga_{0.09}P$ QDs for oxophosphorus from the $GaPO_3$ moiety.[26] Consequently, it may be assigned to the indium counterpart, $InPO_3$, some of these oxygen atoms possibly coming from the capping palmitate ligand. Finally, the minor signal at 48 ppm may correspond to low-coordinated phosphorus atoms (dangling phosphorus): the intensity of this latter resonance disappears when the surface is coated with ZnS.[22]

The presence of oxidized or partially oxidized InP raises the issue of the source of oxidation, since the synthesis and characterization were conducted in air-free devices and all solvents and reagents were rigorously degassed and dried prior use. This prompted us to study, in detail, the mechanism of formation of InP NCs and in particular the surface−ligand composition and the chemistry of the precursors involved in the synthesis.

Surface−Ligand Composition. A combination of spectroscopic techniques was employed to probe the surface environment of the NCs, which contains ca. 77 wt % of organic species as determined by elemental analysis. A FT-IR spectrum of the as-synthesized InP nanoparticles is shown in Figure 3. The first interesting feature is the weak vibrational band with a maximum at 1530 cm^{-1}, which is diagnostic for the presence of carboxylate groups and which is assigned as the carboxyl antisymmetric stretching band of the carboxylate moiety of the palmitate group.[27] Additionally, the IR spectrum exhibits a sharp peak at

(19) Lucey, D. W.; MacRae, D. J.; Furis, M.; Sahoo, Y.; Cartwright, A. N.; Prasad, P. N. *Chem. Mater.* **2005**, *17*, 3754–3762.
(20) Liu, Z.; Kumbhar, A.; Xu, D.; Zhang, J.; Sun, Z.; Fang, Y. *Angew. Chem., Int. Ed.* **2008**, *47*, 3540–3542.
(21) Xu, S.; Kumar, S.; Nann, T. *J. Am. Chem. Soc.* **2006**, *128*, 1054–1055.
(22) Xu, S.; Klama, F.; Ueckermann, H.; Hoogewerff, J.; Claiden, N.; Nann, T. *Sci. Adv. Mater.* **2009**, *1*, 125–137.
(23) Tomaselli, M.; Yarger, J. L.; Bruchez, M.; Havlin, R. H.; de Graw, D.; Pines, A.; Alivisatos, A. P. *J. Chem. Phys.* **1999**, *110*, 8861–8864.
(24) El Hawi, N.; Nayral, C.; Delpech, F.; Coppel, Y.; Cornejo, A.; Castel, A.; Chaudret, B. *Langmuir* **2009**, 7540–7546.
(25) Jasinski, J.; Leppert, V. J.; Lam, S.-T.; Gibson, G. A.; Nauka, K.; Yang, C. C.; Zhou, Z.-L. *Solid State Commun.* **2007**, *141*, 624–627.
(26) Berretini, M. Ph.D. dissertation, University of California, Santa Barbara, 2005.
(27) Nakamoto, K. *Infrared and Raman Spectra of Inorganic and Coordination Compounds*; Wiley-Interscience: New York, 1978; p 232.

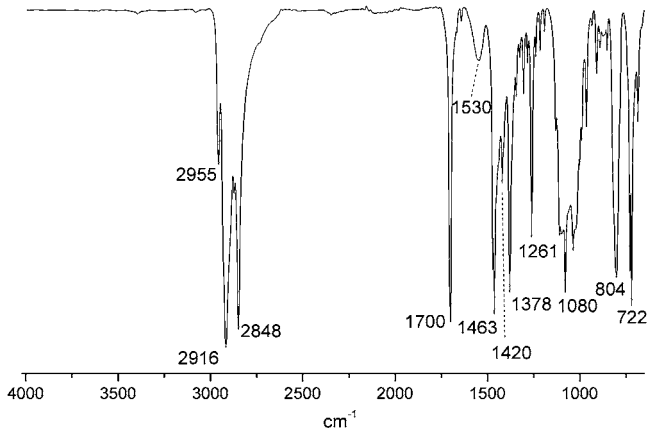

Figure 3. Solid-state FT-IR spectrum of the InP QDs isolated using the standard purifying procedure.

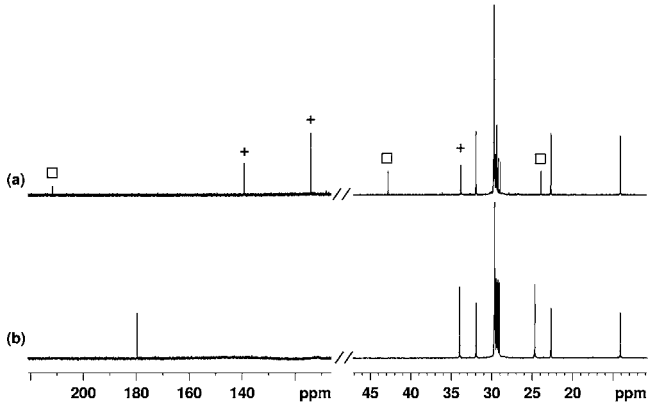

Figure 4. $^{13}C\{^1H\}$ NMR spectra, in $CDCl_3$, of (a) the InP QDs isolated using the standard purifying procedure (□, hentriacontan-16-one; +, ODE) and (b) palmitic acid.

1700 cm^{-1}. This additional band is characteristic of a carbonyl function but does not correspond to any of the starting materials (Figure 3).

The formation of this unknown species is confirmed by the $^{13}C\{^1H\}$ NMR spectrum of the InP QDs suspended in $CDCl_3$. New resonances are observed at δ 211.8, 42.8, and 23.9 ppm (Figure 4a) and suggest the synthesis, during the reaction course, of a symmetrical dialkyl ketone, which is identified as the hentriacontan-16-one, $(C_{15}H_{31})_2CO$, by comparison with the spectroscopic characteristics of a commercial batch of hentriacontan-16-one. The mechanism of formation of this ketone will be discussed in detail in the last section of this article. Along with hentriacontan-16-one characteristic peaks, the solution $^{13}C\{^1H\}$ NMR spectrum also shows the resonances of residual solvent molecules (ODE) (Figure 4). Characteristic resonances are found at δ 139.2 and 114.1 ppm for ethylenic carbons and 33.8 ppm for the methylene carbons located α. Additionally, $^1H-^1H$ COSY, $^1H-^{13}C$ HSQC, and $^1H-^{13}C$ HMBC experiments allow the identification of at least seven isomers of ODE (see Supporting Information, Figure S3). These species were identified by analogy with the chemical shift and the pattern of the very related isomers of 1-nonene. Such a phenomenon is a well-known thermal process which can take place at temperature as low as 110 °C through acid-catalyzed reaction.[28]

Figure 5 shows a typical example of the one-dimensional ^1H NMR spectrum of the as-synthesized InP nanoparticles. As outlined above, it displays the resonances of the palmitate and hentriacontan-16-one molecules and ODE as well as its isomers. It is important to note that their resonances superimpose in the 1.4−0.8 ppm region.

Surprisingly, despite the presence of palmitate ligand supported by the IR spectrum, comparison of the $^{13}C\{^1H\}$ NMR spectrum of these particles with that of palmitic acid (Figure 4b) evidences the absence of the resonances of the carboxylate group. However, when the InP QDs were synthesized using ^{13}C═O-enriched palmitic acid, a broad resonance centered at 183 ppm gave evidence for the presence of carboxylate (see Supporting Information, Figure S4). Despite a high ^{13}C percentage, this peak remains broad and of low intensity. This line broadening is probably due to the decrease of fluxionality of the coordinating function, as previously noted when a surfactant molecule interacted with a nanoparticle surface.[9,10,29,30] Thus, this observation strongly supports the coordination of the carboxylate moiety to the surface of the InP nanoparticle.

As a summary, the capping organic layer is thus composed of a mixture of residual solvent molecules, hentriacontan-16-one, and palmitate coordinated through the carboxylate function.

Surface−Ligand Arrangement. The line shape analysis of the solution $^{13}C\{^1H\}$ NMR spectrum provides significant discrepancies between the very broad palmitate resonance at δ 183 ppm and the narrow ones of hentriacontan-16-one. This prompted us to study in detail their interaction with the InP QDs surface using diffusion-ordered NMR spectroscopy (DOSY) experiments: from the decay of the resonance intensity as a function of field gradient strength of this NMR sequence, the diffusion coefficient of the species associated with the resonance can be obtained. Thus, the resonances of surface-bound ligands and free molecules can be separated along the diffusion dimension of the 2D spectrum if the ligand exchange rate is slow compared to the diffusion time scale.[31] This technique provided, in the particular case of InP with TOP/TOPO ligands, evidence for the presence of both free and bound ligands which are involved in a dynamic equilibrium that is slow with respect to the NMR time scale.[9,31] Similar results were also found for most NMR studies reported so far, i.e., TiO_2, CdSe, or PbSe QDs.[9,10,32,33]

However, in the case of carboxylate-derived InP QDs, the situation contrasts markedly. Only one set of resonances is observed for the palmitate ligand. The bonding is firmly established by DOSY experiments. The self-diffusion coefficient of palmitate has a value of 1.6×10^{-10} m^2/s in QDs, i.e., around 4 times smaller than for the free form (6.8×10^{-10} m^2/s) (Figure 6).

Diffusion coefficients and hydrodynamic radii are correlated by the Stokes−Einstein relation, $D = kT/6\pi\eta r$ (where D is the diffusion coefficient, k is the Boltzmann constant, T is the temperature in K, η is the viscosity of the solution, and r is the radius). Palmitate's self-diffusion coefficient indicates a hydrodynamic diameter of 5.4 nm in chloroform. This value exceeds

(28) Werstiuk, N. H.; Timmins, G. *Can. J. Chem.* **1985**, *63*, 530–533.
(29) Berretini, M. G.; Braun, G.; Hu, J. G.; Strouse, G. F. *J. Am. Chem. Soc.* **2004**, *126*, 7063–7070.
(30) Pan, C.; Pelzer, C.; Philippot, K.; Chaudret, B.; Dassenoy, F.; Lecante, P.; Casanove, M. *J. Am. Chem. Soc.* **2001**, *123*, 7584–7593.
(31) Moreels, I.; Martins, J. C.; Hens, Z. *Sens. Actuators B* **2007**, *126*, 283–288.
(32) Moreels, I.; Fritzinger, B.; Martins, J. C.; Hens, Z. *J. Am. Chem. Soc.* **2008**, *130*, 15081–15086.
(33) Van Lokeren, L.; Maheut, G.; Ribot, F.; Escax, V.; Verbruggen, I.; Sanchez, C.; Martins, J. C.; Biesemans, M.; Willem, M. *Chem. Eur. J.* **2007**, *13*, 6957–6966.

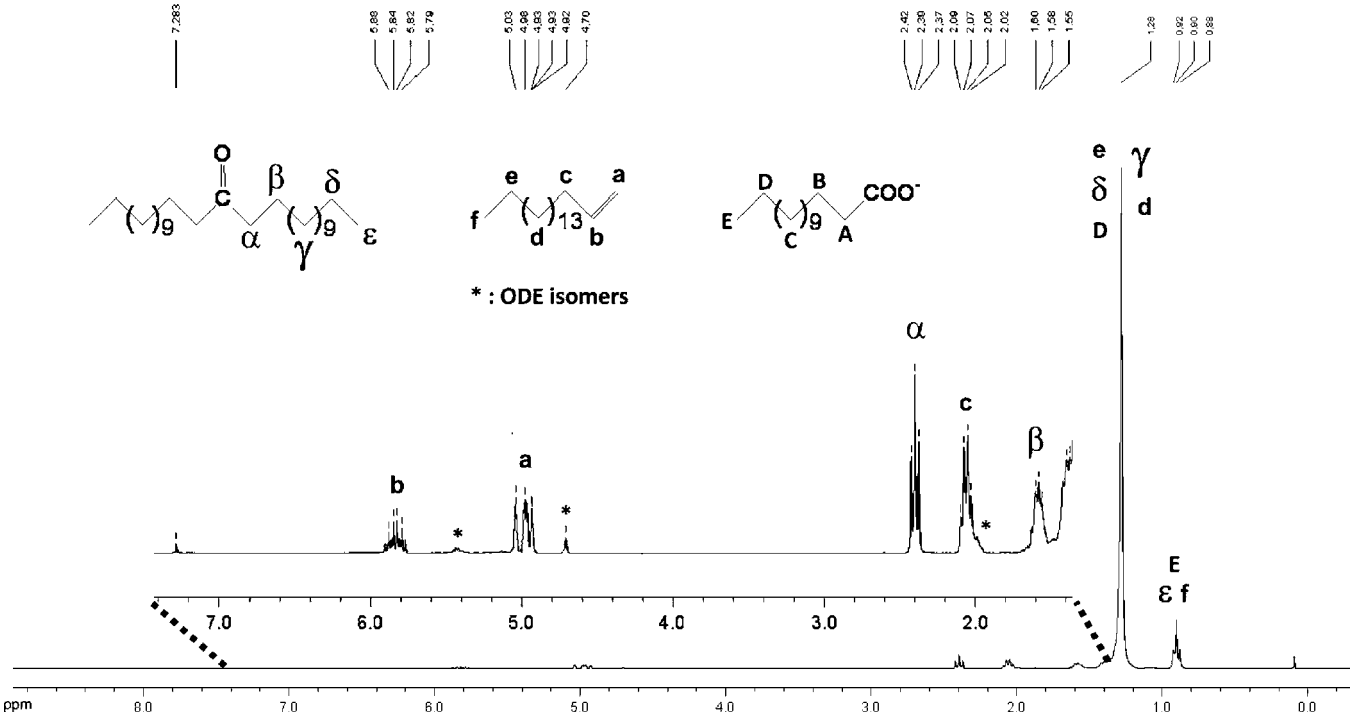

Figure 5. One-dimensional ^{1}H NMR spectrum, in $CDCl_3$, of InP QDs isolated using the standard purifying procedure ([InP QDs] = 2.0×10^{-4} M).

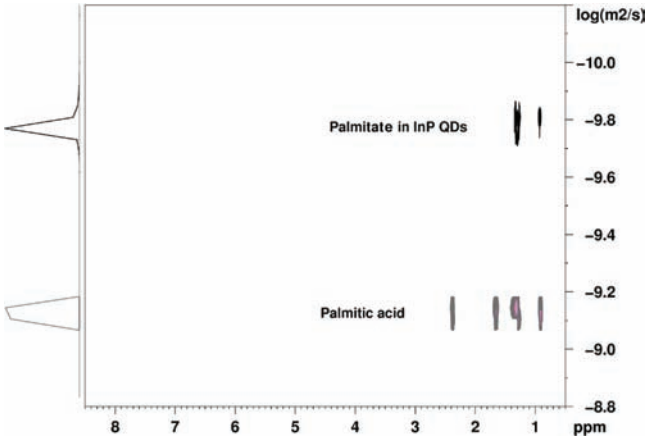

Figure 6. Overlay of 2D DOSY spectra, in $CDCl_3$, of pure palmitic acid and palmitate in InP QDs isolated using the standard purifying procedure.

the NC diameter by ca. 2 nm, which is consistent with the thickness of the palmitate capping layer. The slow diffusion coefficient and the match between the hydrodynamic diameter and QDs core size unambiguously evidence that these ligands are tightly bound to the NCs surface. This confirms the absence of exchange of coordinated carboxylate groups with free species and, thus, discards exchange phenomenon as a potential explanation for the broadening of palmitate NMR signals. It results most probably from residual dipole coupling due to restricted mobility at the interface, as previously observed, and possibly from chemical shift distribution due to a distribution in sites at the nanoparticle interface.[29,30]

Concerning ODE and its isomers, the diffusion coefficients decrease significantly (3.7×10^{-10} vs 10.0×10^{-10} m^2/s for ODE and 2.2×10^{-10} vs 10.0×10^{-10} m^2/s for ODE isomers) in the QDs solution (see Supporting Information, Figure S5). This reduction evidences interaction with the nanoparticles, either with the InP QDs surface or with coordinated palmitate through van der Waals interaction. In both cases, the kinetics of exchange between the free and the interacting states with QDs is fast on the NMR time scale. Thus, only chemical shifts and the population-average diffusion coefficient can be extracted from the DOSY experiment. Recently, Martins et al. have shown that transfer NOE (trNOE) techniques can be successfully used to analyze adsorption/desorption behavior of molecules and to distinguish fast-exchanging ligands which are in contact with the surface from nonligands. Strong negative NOEs are observed if ligands are bound to the NCs surface, while no effect is evidenced for the other situation.[34] When this NMR technique was applied to an InP QDs solution, no negative NOEs involving ODE resonances were observed. Instead zero-quantum coherence (ZQC) cross-peaks at 2.0 and 2.1 ppm, typically recognized from their antiphase line shape, were evidenced and clearly showed that ODE and its isomers are interacting with the palmitate chain rather than the InP surface (Figure 7a). Similarly, the diffusion coefficient of the hentriacontan-16-one decreases in the presence of the InP QDs (see Supporting Information, Figure S6), and ZQC cross-peaks are observed (Figure 7a) for the corresponding resonances at δ 1.6 and 2.3 ppm. However, since this decrease is weak (5.2×10^{-10} vs 5.9×10^{-10} m^2/s), the contribution of a viscosity effect could also account for the variation.

Consistent with palmitate coordination, negative NOEs are observed for the bound palmitate ligand (δ 2.3 ppm) when the threshold of the contour plot is lowered (see Supporting Information, Figure S7). However, the intensity of the cross-peak is weak because of the high concentrations of hentriacontan-16-one and ODE with respect to the carboxylate ligand. For the same reason, the negative NOE cross-peaks of other palmitate resonances are hidden by the correlation peaks of the hentriacontan-16-one and ODE.

(34) Fritzinger, B.; Moreels, I.; Lommens, P.; Koole, R.; Hens, Z.; Martins, J. C. *J. Am. Chem. Soc.* **2009**, *131*, 3024–3032.

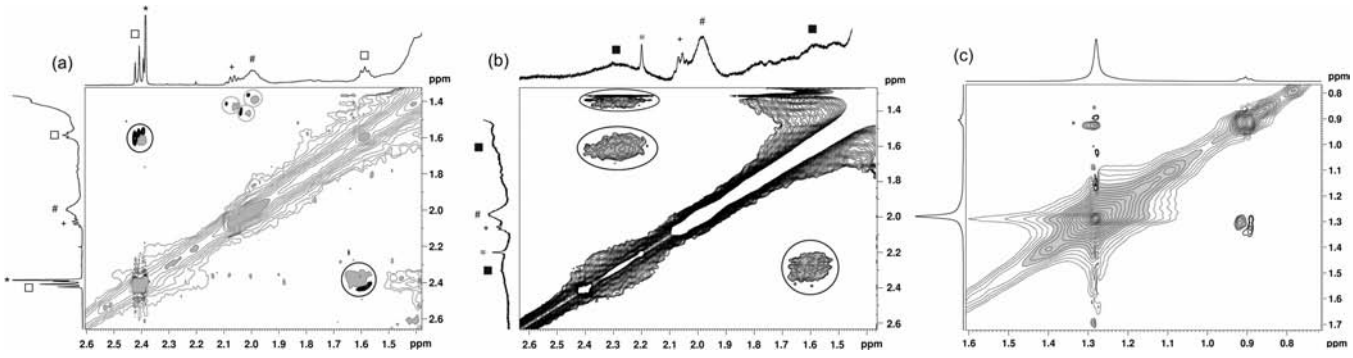

Figure 7. Zooms of the NOESY spectra, in $CDCl_3$, of (a) InP QDs isolated using the standard purifying procedure (□, hentriacontan-16-one; *, residual toluene; +, ODE; #, ODE isomers) in the 1.4−2.6 ppm region, (b) InP QDs isolated using the acetone-based purifying procedure (■, palmitate ligand; *, residual acetone; +, ODE; #, ODE isomers) in the 1.4−2.6 ppm region, and (c) InP QDs isolated using the acetone-based purifying procedure in the 0.7−1.6 ppm region.

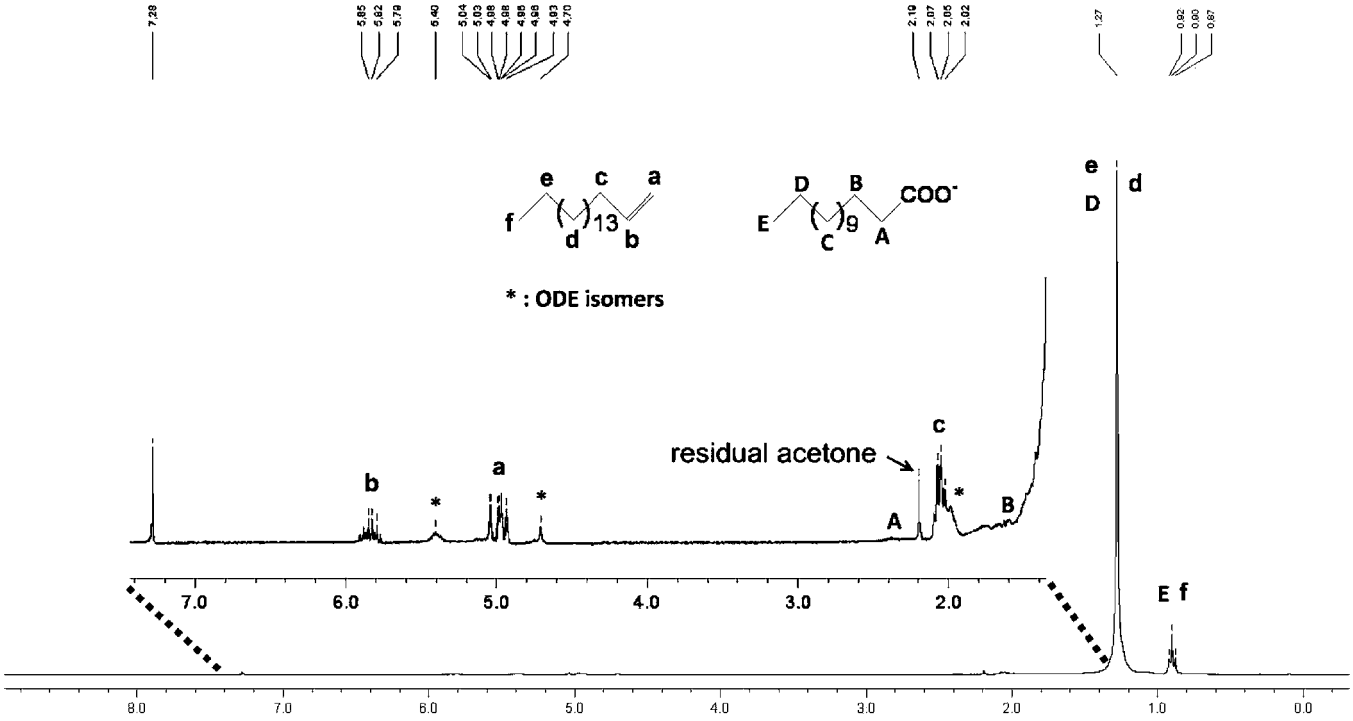

Figure 8. One-dimensional ^1H NMR spectrum, in $CDCl_3$, of InP QDs isolated using the acetone-based purifying procedure ([InP QDs] = 3.6×10^{-4} M).

This prompted us to reconsider the isolation workup. When modifying the precipitation procedure and using a mixture of chloroform and acetone (see Experimental Section, acetone-based purifying procedure), we succeeded in isolating InP QDs free of hentriacontan-16-one, as evidenced by the solution ^1H NMR (Figure 8) and $^{13}C\{^1H\}$ NMR spectra (see Supporting Information, Figure S8) and by the IR spectrum of the as-isolated InP nanoparticles (see Supporting Information, Figure S9). In the latter case, the sole carboxyl antisymmetric and symmetric stretching bands of the carboxylate moiety of the palmitate group (at 1527 and 1442 cm^{-1}, respectively) are observed in the carboxyl frequency range of the IR spectrum.

When the trNOE NMR technique is applied, strong negative NOEs are observed for α-CH_2 (2.3 ppm) and β-CH_2 (1.6 ppm) resonances (Figure 7b), confirming the coordination of the palmitate. In contrast to previous observations,[35] no negative NOEs are visible for the CH_3 group at the extremity of the palmitate alkyl chain (Figure 7c), presumably because of a high tumbling motion of the alkyl chain far from the surface. ODE and its isomers that are not interacting directly with the QD surface are probably also very mobile, and this may explain why we could not observe negative NOEs on these molecules.

Thus, these spectroscopic data clearly evidence that the palmitate molecules are the sole ligand and coordinate firmly the indium-rich QDs surface, ensuring at the same time the colloidal stability. In parallel, they also interact with ODE and possibly hentriacontan-16-one via weak interchain interactions. A graphical schematic representation summarizing the core−multishell structure (core, InP; shell 1, $InPO_x$; shell 2, palmitate ligand; shell 3, hentriacontan-16-one and ODE isomers) is given in Figure 9.

Bonding Mode and Quantification of the Palmitate Ligand. In the literature, basically four different metal−ligand coordination types are discussed: the carboxylate can act as an uncoordinated

(35) Fritzinger, B.; Capek, R. K.; Lambert, K.; Martins, J. C.; Hens, Z. *J. Am. Chem. Soc.* **2010**, *132*, 10195–10201.

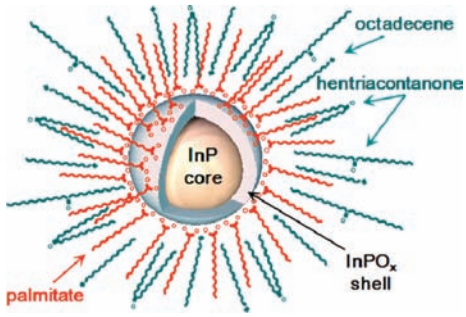

Figure 9. Graphical schematic representation of InP QDs isolated using the standard purifying procedure.

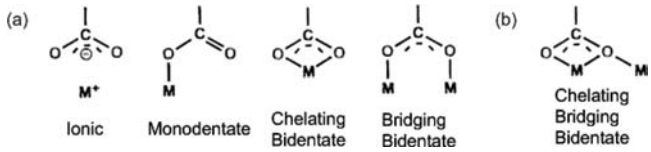

Figure 10. (a) Basic carboxylate binding modes and (b) additional carboxylate binding mode observed in indium carboxylate complexes.

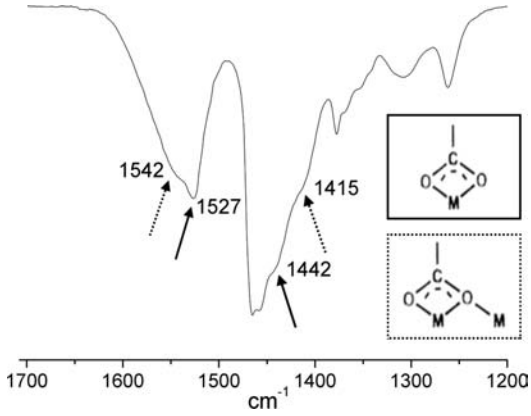

Figure 11. Solid-state FT-IR spectrum of the InP QDs isolated using the acetone-based purifying procedure. The two palmitate bonding modes are evidenced by solid arrows for the chelating bidentate coordination and by dashed arrows for the chelating bridging bidentate coordination.

anion ("ionic" structure) or form a monodentate ligand, a bidendate chelate, or a bridging bidentate structure (Figure 10a).

It is possible to qualitatively distinguish the coordination modes by IR spectroscopy, based on the frequency difference between the antisymmetric and symmetric $\nu(CO_2^-)$ stretches.[27,36] The difference between these two stretching energies (85 cm^{-1}) in the as-synthesized InP QDs supports a chelating coordination mode for the palmitate (Figure 11).

However, the asymmetry and the width of these two bands may also indicate the possible existence of more than one component, i.e., more than a symmetrically bidentate chelating coordination (Figure 11). The carbonyl ^{13}C NMR chemical shift of the carboxylate ligand has been shown to be a highly sensitive probe to diagnose, with high resolution, the binding modes of the carboxylate.[37−39] Both the NMR and the IR data of the InP NCs show strong similarities with those of the complex In(palm)$_3$: the IR spectra reveal almost identical line shapes (see Supporting Information, Figure S10), and the NMR spectra in the carbonyl chemical shift range (see Supporting Information, Figure S11) display two resonances at δ 183.0 and 183.8 ppm (for the palmitate-capped InP QDs, a broad resonance is centered on 183 ppm, with a width at half-height of 3 ppm). Thus, these results strongly support that a similar coordination chemistry exists at the surface of the InP QDs and in the coordination sphere of the indium atom of In(palm)$_3$.

The well-documented chemistry of indium carboxylates features polynuclear structures, $[In(O_2CR)_3]_n$, in which carboxylate ligands can display either a chelating coordination mode (Figure 10a) or a chelating bridging bidentate one (Figure 10b) in which the carboxylate chelates asymmetrically the metal center, with one of the oxygen atoms bridging the next indium atom.[40] In the case of In(palm)$_3$, the $^{13}C\{^1H\}$ MAS NMR spectrum (two carbonyl resonances at δ 183.0 and 183.8 ppm) is in perfect agreement with these two possible arrangements of carboxylates.

Furthermore, switching to other bonding modes, such as the true bridging bidentate one (Figure 10a), would have resulted in at least a 5 ppm shift.[37,39] It is thus reasonable to describe the coordination of palmitate at the surface of InP QDs as predominantly chelating to indium, with secondary bridging interactions with neighboring atoms (In and/or P). These latter interactions may be invoked to account for the broadening of the NMR carboxylate resonance and the antisymmetric and symmetric C−O stretchings in the IR data.

The organic capping species which go along with the InP core have been quantified, thanks to IR data.[41] Knowing the InP QDs concentration,[42] an average density of four palmitate ligands per square nanometer of InP QDs surface was calculated. This coverage density is comparable to that found for TOPO in TOP/TOPO-based synthesis of InP QDs and for oleic acid in PbSe NCs.[10,32]

Concerning the possible interactions between the alkyl chain of the palmitate ligands, IR spectroscopy measurements probe molecular vibration occurring on a time scale shorter than 10^{-10} s and provide a "snapshot" of the different bond conformations existing at a given instant. In a $CDCl_3$ solution of InP QDs, the symmetric and antisymmetric (CH_2) stretching modes are observed at 2854 and 2927 cm^{-1}, respectively, consistent with assignment of a disordered arrangement, as in the *n*-alkane melts (Figure 12a).[43] However, in the solid state, for the isolated InP QDs, the line width of these bands decreases, and there is a shift to lower frequencies (2850 and 2918 cm^{-1}, respectively) (Figure 12b).[44] This can be attributed to a predominantly all-*trans* packing arrangement of the ligands at the surface. Thus, these latter pack and behave as a condensed-phase monolayer in a solid state.[45] This is consistent with the closed-packed arrangement and the short interparticle distance of the InP/ZnS QDs observed by Reiss et al.[46]

(36) Deacon, G. B.; Phillips, R. J. *Coord. Chem. Rev.* **1980**, *33*, 227–250.
(37) Ye, B.-H.; Li, X.-Y.; Williams, I. D.; Chen, X. M. *Inorg. Chem.* **2002**, *25*, 6426–6431.
(38) Ribot, F.; Toledano, P.; Sanchez, C. *Inorg. Chim. Acta* **1991**, *185*, 239–245.
(39) Uhl, W.; Graupner, R.; Hahn, I. *Z. Anorg. Allg. Chem.* **1997**, *623*, 565–572.
(40) Lindel, W.; Huber, F. *Z. Anorg. Allg. Chem.* **1974**, *408*, 167–174.
(41) Ramsay, D. A. *J. Am. Chem. Soc.* **1952**, *74*, 72–80.
(42) Reiss, P.; Protière, M.; Li, L. *Small* **2009**, *5*, 154–168.
(43) Snyder, R. G.; Strauss, H. L.; Ellinger, C. A. *J. Phys. Chem.* **1982**, *86*, 5145–5151.
(44) MacPhail, R. A.; Strauss, H. L.; Snyder, R. G.; Ellinger, C. A. *J. Phys. Chem.* **1984**, *88*, 334–341.
(45) Meulenberg, R. W.; Strouse, G. F. *J. Phys. Chem. B* **2001**, *105*, 7438–7445.
(46) Thuy, U. T. D.; Thuy, P. T.; Liem, N. Q.; Li, L.; Reiss, P. *Appl. Phys. Lett.* **2010**, *96*, 073102.

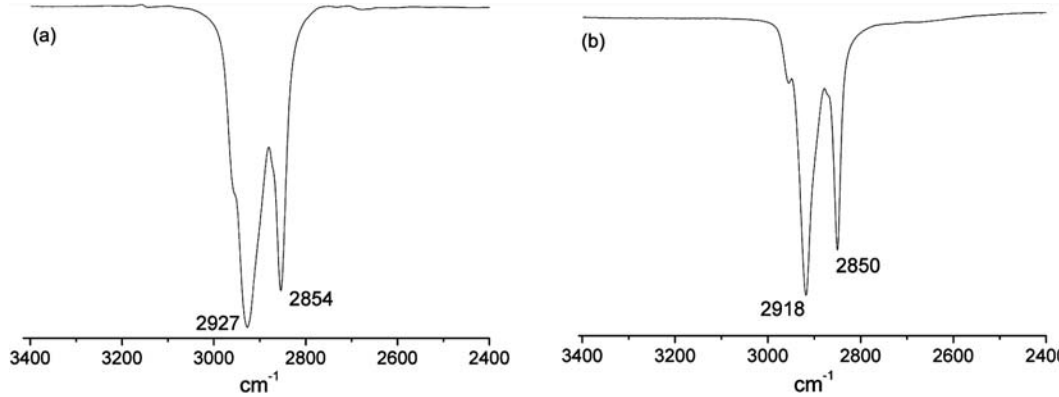

Figure 12. FT-IR spectra of the InP QDs isolated using the acetone-based purifying procedure (a) in $CDCl_3$ and (b) in solid-state.

Precursors' Reactivity and Surface Chemistry of the InP Nanocrystals. The FT-IR and NMR analyses have demonstrated the formation of the hentriacontan-16-one, $(C_{15}H_{31})_2CO$, presumably through the decarboxylative coupling (ketonization) of palmitic acid, releasing water and carbon dioxide as byproducts.[47]

Monitoring of the reaction mixture and in particular the carbonyl compounds during the whole procedure has been realized (Figure 13). The first step involves heating $In(OAc)_3$ in the presence of 3 equiv of palmitic acid. This latter quantity is just the sufficient amount to replace all acetate. However, as previously noted,[48] the ligand replacement does not go to completion. Using FT-IR peaks,[41] we show that 7% of the introduced palmitic acid remains unconverted at 200 °C. Upon heating to 300 °C, this amount decreases to ca. 1%. The CO vibration band of hentriacontan-16-one starts to be detectable at 300 °C, but quantification reveals that its quantity remains very low (approximately 1% of the expected amount in the case of total conversion of the introduced palmitic acid). Upon injection of $P(TMS)_3$ at 300 °C, and thus during the nucleation step, the IR spectrum clearly shows the production of a significant amount of hentriacontan-16-one: 25% of all the palmitate molecules have been converted. Decarboxylative coupling proceeds all through the reaction: after 1 h, more than 55% of the palmitate molecules have been converted to ketones (Figure 13).

Concerning the identification of the species responsible for the ketonization, no hentriacontan-16-one formed when palmitic acid was heated alone at 300 °C, nor in the presence of In_2O_3 nanoparticles (which are sometimes observed as minor byproduct during the synthesis of InP QDs).[22] As stated above, minor formation of hentriacontan-16-one is observed in the presence of indium carboxylates, but this reaction requires a longer reaction time to efficiently convert palmitic acid into appreciable amounts of hentriacontan-16-one. Thus, these results evidence that ketone formation goes along with the formation of the InP QDs.

Consistent with the occurrence of ketonization, Karl Fischer titration confirms the parallel formation of water as a side product. The reactivity of water with InP NCs was thus evaluated. The addition to the as-synthesized InP QDs of 1.5 equiv of water, compared to introduction of palmitic acid, at 280 °C results in surface oxidation of the surface NCs, as

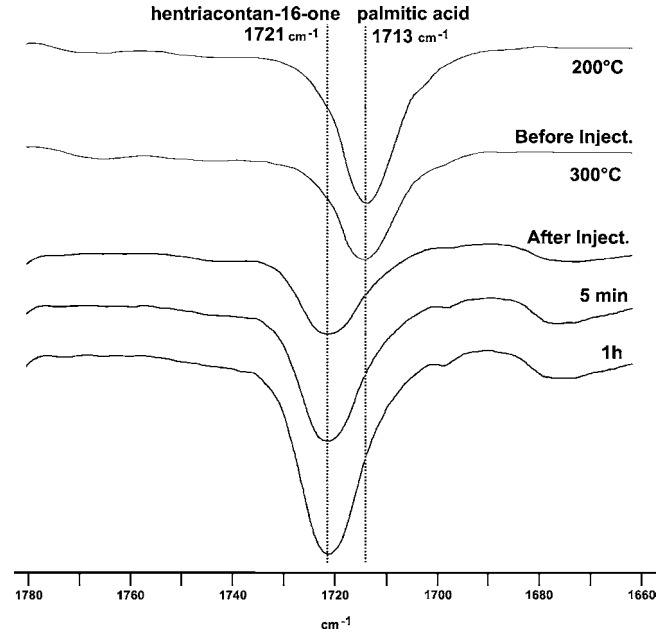

Figure 13. Temporal evolution of the FT-IR spectrum for the reaction mixture of the InP QDs.

evidenced by the $^{31}P\{^1H\}$ MAS NMR spectrum of the resulting nanoparticles (Figure 14a). The same four resonances are observed; however, the $^{31}P\{^1H\}$ MAS NMR spectrum clearly shows a significant increase in the ratio of phosphorus atoms from phosphate ($In^{31}PO_4$), which almost doubles (from 12% to 22%), while that of the $In^{31}P$ signal significantly decreases from 82% to 71% (Figure 14a and see Supporting Information, Figure S12). Interestingly, this also results in important modifications of the $In^{31}P$ resonances: on one hand, the chemical shift moves to δ −204 ppm (vs −214 ppm before water addition), and on the other hand the line shape shows a significant narrowing (more than 20%) of the corresponding signal ($\delta_{1/2} = 55$ ppm). These observations are comparable to the results observed when the InP core is coated with higher band gap semiconductors such CdS (see Supporting Information, Figure S13) and suggest the formation of $InP/InPO_x$ core−shell nanoparticles.

The optical properties of the InP QDs were also found to be dramatically modified, in particular with the high increase in the band edge luminescence intensity and the strong decrease of the surface defect emission (Figure 14b). Previous studies[16,49]

(47) Renz, M. *Eur. J. Org. Chem.* **2005**, 979–988.
(48) Narayanaswamy, A.; Xu, H.; Pradhan, N.; Kim, M.; Peng, X. *J. Am. Chem. Soc.* **2006**, *128*, 10310–10319.

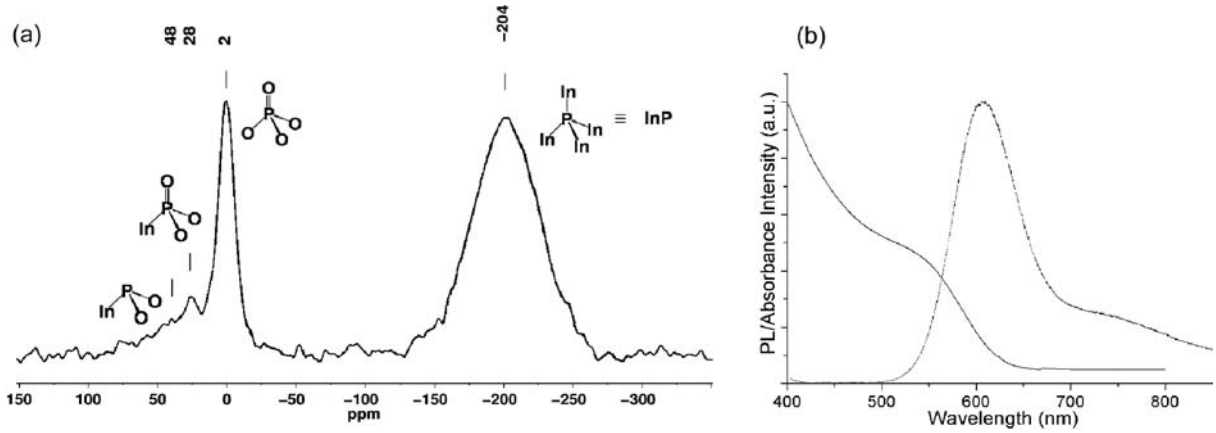

Figure 14. (a) $^{31}P\{^{1}H\}$ MAS NMR and (b) UV−vis and PL spectra of InP QDs after water injection.

have also shown that a surface oxide layer enhances the photoluminescence quantum yields by 1 order of magnitude.

Discussion

The major advance reported in this article is the role of palmitate molecules, which go beyond the expected function of capping ligand. Indeed, they are involved in the organic side reaction leading to the hentriacontan-16-one formation. A reasonable hypothesis is that, at high reaction temperatures, two palmitic acid molecules condense to form the corresponding ketone, a reaction called decarboxylative coupling or ketonization. The ketonization of carboxylic acids has been a familiar reaction in organic chemistry for more than a century: two carboxylic acid molecules with n carbon atoms are converted, at a temperature of about 300−400 °C, into a symmetrical ketone with $2n - 1$ carbon atoms, releasing CO_2 and H_2O during the process.[47] Regarding the potential mechanism, previous reports describe that it may occur at high temperature (300 °C) without the assistance of any adjuvant or in the presence of either solid metal oxides or carboxylate salts of divalent or higher-valent cations.[47,50] In our case, significant amounts of the hentriacontan-16-one form only in the presence of the InP QDs. Thus, these results evidence that ketone formation goes along with the formation of the InP QDs.

In the past few years, several research groups have started to investigate the molecular mechanisms of the precursor and the chemical transformations of the organic components in the synthesis of NCs, but these studies have remained limited to II−VI[51,52] and IV−VI[53] derived materials. These reactions are found to be crucial in these surfactant-directed synthesis routes with a high content of organic compounds: the first results demonstrate that the manifold role of surfactant is more complex than originally anticipated and provide a step forward in the understanding of particle formation.[54] Indeed, ligands are involved in every step of the synthetic process and in particular as reagents in the conversion of precursor molecules to semiconductor materials.[51] As a relevant example of the benefits in terms of control of such studies, the surface−ligand composition of CdSe NCs prepared using TOPO was investigated and showed the presence of *n*-octylphosphonic acid, which forms *in situ* and plays the main role in the growth and stabilization of these nanoparticles.[55−57] Analogously, systematic analysis of the formation mechanism of PbSe QDs evidenced that the presence of even trace amounts of acetate group in the reaction mixture leads to starlike geometries formed by oriented attachment.[58] Identification and quantification of organic byproducts (present in the starting solution or formed *in situ* during the reaction course) have thus, on one hand, provided valuable information about the chemical reaction mechanisms[59] and, on the other hand, influenced to a great extent the final characteristics of the QDs, even if they are present in a small amount. In our case, the hentriacontan-16-one plays a minor role in terms of capping ligand activity, and a well-designed washing procedure gets rid of it. Nevertheless, the formation of this ketone is far from being innocent in the reaction pathway. It occurs with QDs formation and leads to concomitant water release. Although the role of water has been carefully analyzed and shown to be essential in many cases, such as in the synthesis of In_2O_3 from indium carboxylates in ODE,[48] to the best of our knowledge, no detailed study has ever been conducted for InP QDs. In our case, ^{31}P MAS NMR experiments and photoluminescence studies give consistent results showing that the presence of water leads to oxidation of the InP NCs surface, i.e., to an InP/$InPO_x$ core−shell structure. Thus, these data show that ketonization provides oxidative conditions, which obviously greatly impact the chemical and physical properties of the InP NCs. These new elements hint at a rationale for the failure of growing InP NCs using this synthetic route (i.e., fatty acid as stabilizer and ODE as solvent): it is very likely that the formation of a partially oxidized shell deactivates InP growth whatever the mechanism involved.[17] Therefore, this raises the question of the pertinence of the use of carboxylic acid/carboxylate

(49) Guzelian, A. A.; Katari, J. E. B.; Kadavanich, A. V.; Banin, U.; Hamad, K.; Juban, E.; Alivisatos, A. P.; Wolters, R. H.; Arnold, C. C.; Heath, J. R. *J. Phys. Chem.* **1996**, *100*, 7212–7219.
(50) Patai, S. *The chemistry of the carbonyl group*; Interscience: London, 1966; p 211.
(51) Liu, H.; Owen, J. S.; Alivisatos, A. P. *J. Am. Chem. Soc.* **2007**, *129*, 305–312.
(52) Xi, L.; Tan, W. X. W.; Boothroyd, C.; Lam, Y. M. *Chem. Mater.* **2008**, *20*, 5444–5452.
(53) Steckel, J. S.; Yen, B. K. H.; Oertel, D. C.; Bawendi, M. G. *J. Am. Chem. Soc.* **2006**, *128*, 13032–13033.
(54) Garnweitner, G.; Niederberger, M. *J. Mater. Chem.* **2008**, *18*, 1171–1182.
(55) Kopping, J. T.; Patten, T. E. *J. Am. Chem. Soc.* **2008**, *130*, 5689–5698.
(56) Wang, F.; Tang, R.; Kao, J.L.-F.; Dingman, S. D.; Buhro, W. E. *J. Am. Chem. Soc.* **2009**, *131*, 4983–4994.
(57) Owen, J. S.; Park, J.; Trudeau, P.-E.; Alivisatos, P. A. *J. Am. Chem. Soc.* **2008**, *130*, 12279–12281.
(58) Houtepen, A. J.; Koole, R.; Vanmaekelbergh, D.; Meeldijk, J.; Hickey, S. G. *J. Am. Chem. Soc.* **2006**, *128*, 6792–6793.
(59) Niederberger, M. *Acc. Chem. Res.* **2007**, *40*, 793–800.

precursors in such syntheses. More generally, this issue is of dramatic importance for the design of highly efficient luminescent materials, because uncontrolled phase formation may result in uncontrolled optical properties (quantum yield, size-controlled emission wavelength).

Conclusion

This work provides a comprehensive overview of the surface environment and chemistry of the InP QDs prepared via an indium carboxylate-based route. Using a combination of spectroscopic techniques (in particular, IR and solution and solid-state ^{1}H, ^{13}C, and ^{31}P NMR) that allows a detailed description of the structure and dynamics at the molecular scale, we have shown that these QDs display an InP/$InPO_x$/palmitate core−shells structure. The ligand palmitate is firmly coordinated at the surface, whereas ODE and possibly hentriacontan-16-one interact via weak interchain interactions and can be removed from the coordination sphere via an appropriate washing procedure. The surface oxidation of the InP core is a direct consequence of the synthetic strategy which involves carboxylate ligands: during the QDs formation step, they condense to form the corresponding ketone (the hentriacontan-16-one $(C_{15}H_{31})_2$-CO) and provide oxidative conditions. This partial oxidation is inextricably linked to the involvement of carboxylic acids; thus, a similar oxidation phenomenon is expected when following this synthetic route. It is therefore very likely that the formation of this oxide could prevent further growth of the InP core, the surface being then deactivated for the ripening process. As a consequence, this synthesis method yields small core−shell InP particles. More generally, and given the central and ubiquitous role played by carboxylic acids in the synthesis of NCs, the issue of oxidation is raised with evidence and may thus deserve particular attention for the understanding and the control of the physical and chemical properties of the as-synthesized NPs. Therefore, the development of rational synthesis strategies requires a detailed overview of the roles played by all the components, i.e., the starting organic and inorganic compounds, at the molecular level. This implies a better knowledge of the surface−ligand and ligand−ligand interactions but also the chemical transformations occurring during the synthesis of NCs.

Acknowledgment. A.C.G. is grateful to the Ministère de l'Enseignement Supérieur et de la Recherche for a fellowship. A.C. is grateful to the Spanish Ministerio de Ciencia e Innovacion for a postdoctoral grant. This work was supported by the Université Paul Sabatier, the Région Midi-Pyrénées, the CNRS, and the Institut National des Sciences Appliquées of Toulouse. We thank Laure Vendier for XRD measurements and Thomas Belhadj and Bernhard Urbaszek for assistance with PL measurements. We thank Angélique Gillet for helpful work.

Supporting Information Available: Deconvoluted $^{31}P\{^{1}H\}$ MAS NMR spectrum of InP QDs isolated using the standard purifying procedure; $^{31}P\{^{1}H\}$ MAS NMR spectra of InP QDs exposed to air for 45 days; $^{1}H-^{13}C$ HMBC, $^{1}H-^{13}C$ HSQC, and $^{1}H-^{1}H$ COSY NMR spectra in $CDCl_3$ of InP QDs (ethylenic region) isolated using the standard purifying procedure; $^{13}C\{^{1}H\}$ NMR spectrum in $CDCl_3$ of InP QDs incorporating ^{13}C═O-enriched palmitate ligand; overlay of 2D DOSY spectra in $CDCl_3$ of pure ODE and ODE and its isomers in InP QDs (i.e., isolated using the standard purifying procedure); overlay of 2D DOSY spectra in $CDCl_3$ of pure hentriacontan-16-one and hentriacontan-16-one in InP QDs (i.e., isolated using the standard purifying procedure); NOESY spectra in $CDCl_3$ of InP QDs isolated using the standard purifying procedure (low threshold of the contour plot); $^{13}C\{^{1}H\}$ NMR spectra in $CDCl_3$ of the InP QDs isolated using the acetone-based purifying procedure; solid-state FT-IR spectrum of the InP QDs isolated using the acetone-based purifying procedure; comparison of the solid state FT-IR spectra of $In(palm)_3$ and the InP QDs isolated using the acetone-based purifying procedure; $^{13}C\{^{1}H\}$ MAS NMR spectrum of $In(palm)_3$; $^{31}P\{^{1}H\}$ MAS NMR spectra of InP QDs after water injection; $^{31}P\{^{1}H\}$ MAS NMR spectra of InP/CdS QDs; ^{1}H NMR of palmitic acid in $CDCl_3$; ^{1}H NMR of hentriacontan-16-one in $CDCl_3$. This material is available free of charge via the Internet at http://pubs.acs.org.

JA104673Y